

Impact of CCN hygroscopicity and turbulence on cloud droplet growth: An in-cloud seeding case study using a parcel-DNS approach

Sisi Chen^{1,2}, Lulin Xue¹, and Man-Kong Yau²

¹National Center for Atmospheric Research, Boulder, Colorado, USA

²McGill University, Montréal, Québec, Canada

Correspondence: Sisi Chen (sisichen@ucar.edu)

Abstract.

This paper investigates the relative importance of turbulence and aerosol effects on the broadening of the droplet size distribution (DSD) during the early stage of cloud and raindrop formation. A parcel-direct numerical simulation (DNS) hybrid approach is developed to seamlessly simulate the evolution of cloud droplets in an ascending cloud parcel. The results show that turbulence and CCN hygroscopicity are key to the efficient formation of large droplets. The ultra giant aerosols can quickly form embryonic drizzle drops and thus determines the onset time of autoconversion. However, due to their scarcity in natural clouds, their contribution to the total mass of drizzle drops is insignificant. In the meantime, turbulence sustains the formation of large droplets by effectively accelerating the collisions of small droplets. The DSD broadening through turbulent collisions is significant and therefore yields a higher autoconversion rate compared to that in a non-turbulent case. It is argued that the level of autoconversion is heavily determined by turbulence intensity. This paper also presents an in-cloud seeding scenario designed to scrutinize the effect of aerosols in terms of number concentration and size. It is found that seeding more aerosols leads to higher competition for water vapor and reduces the mean droplet radius, and therefore slows down the autoconversion rate. on the other hand, increasing the seeding particle size can buffer such negative feedback. Despite that the autoconversion rate is prominently altered by turbulence and seeding, parcel-mean variables such as LWC stays nearly identical among all cases. Additionally, the lowest autoconversion rate is not co-located with the smallest mean droplet radius. The finding indicates that the traditional Kessler-type or Sundqvist-type autoconversion parameterizations which depend on the LWC or mean radius could not well-capture the drizzle formation process. Properties related to the width or the shape of the DSD are also needed, suggesting that the Berry-and-Reinhardt scheme is conceptually better. It is also suggested that a turbulence-dependent relative-dispersion parameter should be considered.

20 *Copyright statement.* The work is original and has not been formally published before, that it is not under the consideration for publication elsewhere. This is an Open Access article distributed under the terms of the CC BY License 4.0.

1 Introduction

Aerosol-cloud-precipitation interactions represent one of the major uncertainties in weather and climate prediction (Fan et al., 2016). Current atmospheric models can not resolve the microphysical processes and thus rely on parameterizations to represent those interactions. Studies show that model results of the location and intensity of precipitation are sensitive to microphysics schemes (Xue et al., 2017; White et al., 2017; Grabowski et al., 2019). For example, White et al. (2017) showed that the autoconversion scheme is the dominant factor to account for the difference in rain production, and the uncertainty due to the choice of microphysical parameterizations exceeds the effects of aerosols. Up to this date, no benchmark “truth” from either measurements or modeling exists to gauge the performance of various microphysics schemes. On the one hand, in-situ measurements cannot directly obtain the process rates, such as the rate of autoconversion and accretion, which prevents such microphysical processes from being accurately modeled. The community has to rely on laboratory experiments, indirect observations, or theoretical models to develop and validate microphysical schemes (e.g., Stoelinga et al., 2003; Wood et al., 2002; Wang et al., 2005). On the other hand, laboratory facilities such as cloud chambers are difficult to create environments scalable to real clouds. Furthermore, the effects of chamber walls, such as the heat and moisture fluxes fed into the solid wall and the droplet loss due to their contact with the wall, are challenging to quantify with considerable uncertainties in the measurements. For example, Thomas et al. (2019) used a flux-balance model to estimate the wall effect on the mean temperature and mean water vapor mixing ratio and found that the results highly depend on the geometry of the chamber.

Currently, direct numerical simulation (DNS) is believed to be the only numerical approach capable of simulating the growth of individual cloud particles in turbulent flows (Grabowski et al., 2019). Only a few DNS studies to date investigated the evolution of the droplet size distribution (DSD) in an updraft environment (e.g., Chen et al., 2018b; Gotoh et al., 2016; Saito and Gotoh, 2018). However, the solute effect (aerosol hygroscopicity) and curvature effect were excluded in those works for simplicity. Other DNS studies focused on the steady-state conditions, i.e., zero updrafts with zero mean supersaturation (e.g., Li et al., 2020; Sardina et al., 2015). It is recognized that DNS is computationally expensive. To achieve an accurate representation of cloud microphysics while maintaining a feasible computational load, a hybrid modeling framework that combines a parcel model and a DNS model is proposed in this study. The parcel model provides the mean state of the air parcel and can be used when the effect of turbulence is less prominent. The DNS model explicitly resolves all small-scale turbulent eddies which are key to cloud particle interactions. The Lagrangian particle method is employed in the DNS to track the evolution of individual cloud particles coupling with the turbulent flow. This hybrid parcel-DNS approach allows a close examination of the growth history of cloud particles from aerosol activation to drizzle formation. By comparing simulations with different aerosol and turbulent conditions, we are able to evaluate the contribution of each microphysical component to warm rain initiation. The ultimate goal is to provide a numerical benchmarking tool to better understand aerosol-cloud-precipitation interaction at fine scales and improve the sub-grid-scale representation of clouds and precipitation in numerical weather and climate prediction.

Chen et al. (2018b) found that the evolution of DSD in turbulence is different depending on whether droplets grow by condensation-only, collision-only, or condensation-collision (Fig. 1 in their paper). This reveals that droplet condensation and collisions when interacting with turbulence, cannot be treated as the linear addition of the two processes. Many past DNS

studies focused on either the condensation-only process or the collision-only process which might yield biased results. It should be pointed out that autoconversion defined as the mass transfer from small droplets to embryonic drizzle drops via collision-coalescence should not exclude the impact of condensational growth, as the two processes dynamically interact with each other. This paper presents a sequel to the study of Chen et al. (2018b) by addressing several caveats mentioned in their paper. Firstly, Chen et al. (2018b) treated only pure water droplets as is commonly assumed in most DNS studies (e.g., Sardina et al., 2015; Vaillancourt et al., 2001, 2002; Paoli and Shariff, 2009). This simplification may underestimate the rate of droplet growth by condensation. Jensen and Nugent (2017) found that cloud condensation nuclei (CCN) strongly enhances the particle growth, and droplets with giant CCN can even grow in regions of sub-saturated downdrafts. In our new hybrid approach, we use an accurate droplet diffusional growth equation including both curvature effect and solute effect. Secondly, the initial DSD in Chen et al. (2018b) obtained from flight observations was a result of averages over a long-time period and along a long sampling path (including both core regions and cloud edges). The average might mask the local property of an adiabatic core that the DNS aims to simulate. The adiabatic cores are regions free of entrainment of dry air. This region has a higher liquid water content (LWC) than the rest of the cloud and is argued to favor the formation of raindrops (Khain et al., 2013). To represent the DSD evolution at the core region, we prescribe here a dry aerosol size distribution in the sub-cloud region, and the aerosol activation process is explicitly simulated by a parcel model to provide a more physically-based initial DSD for the DNS.

The main purpose of the present study is to investigate the relative importance of turbulence, CCN hygroscopicity and aerosols (size and number concentration) on the DSD broadening in cumulus clouds. The paper is organized as follows. Sections 2.1-2.2 introduce the hybrid model of a parcel-DNS framework, to seamlessly simulate early cloud development from aerosol activation to cloud droplet growth. In Section 2.3, the configuration of the 12 numerical simulations are described to compare the microphysical responses to turbulence (turbulent vs non-turbulent), hygroscopicity (pure-water droplets vs CCN-embedded droplets), aerosol size and number concentration (with or without extra aerosols injected), and droplet growth mechanisms (condensation-only vs condensation-collision). Results are presented in Section 3, showing that turbulence and CCN hygroscopicity are key to the formation of big droplets, and seeding slows down the broadening and lowers the autoconversion rate. Summary and outlook for future work are in Section 4.

2 Model setup

A hybrid model is used in this paper for simulating the droplet growth inside an ascending cloud parcel. The ascending process is divided into two phases based on the distinct dominant microphysical processes. A parcel model and a DNS model are combined to seamlessly simulate the two phases, as illustrated in the schematic diagram in Fig. 1. The first phase starts from the unsaturated sub-cloud region (≈ 300 m below cloud base) to the level where the supersaturation reaches a maximum (≈ 43 m above cloud base, see Fig. 2(a)). During this phase, supersaturation increases with height, and the microphysical process is dominated by aerosol activation. Cloud particles remain small and collisional growth is negligible. A non-turbulent parcel model is employed to calculate the droplet growth by condensation in this phase. The second phase starts from the

level of maximum supersaturation ($\approx 1.59\%$) to 1 km above which takes 500 sec in simulated time (Table 1). At this stage, no new activation occurs as the supersaturation starts to decrease with height. This phase is dominated by cloud droplet growth, and aerosol activation is unimportant. DNS model is employed to calculate individual droplet growth by condensation and collision affected by its immediate local turbulent environment. Outputs from the parcel model at the height with maximum supersaturation are fed into DNS as initial conditions. Because unactivated aerosols have little influence on the subsequent droplet growth or on the water vapor field, only the activated aerosols from the parcel model are carried over to the DNS model as the initial background aerosol condition to decrease the computational load. The CCN size distribution and droplet size distribution are displayed in Fig. 2(c). This parcel-DNS hybrid model provides an economical approach and is the first step towards a fully DNS-resolved simulation of the entire ascending process.

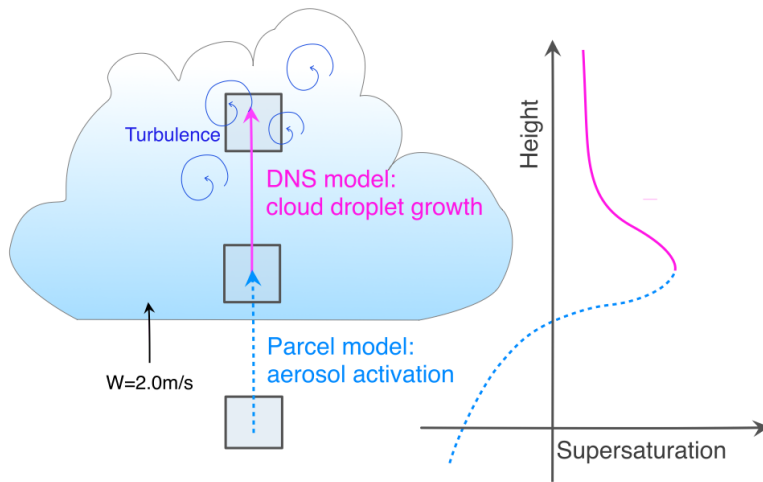


Figure 1. Schematic diagram of the parcel-DNS hybrid model along with the unscaled parcel-mean supersaturation with height. The parcel model simulates the ascending process below the height of maximum supersaturation (dashed blue line), and the DNS simulates the subsequent ascending process (solid violet line).

2.1 Parcel model

The parcel model is adopted from Jensen and Nugent (2017) with two main modifications: (1) The droplet collision-coalescence is excluded for simplicity because most particles in this phase are smaller than $10 \mu m$. These droplets have very small collision rates even in strong turbulence (Chen et al., 2016, 2018a), and the growth is dominated by condensation. (2) The hygroscopicity

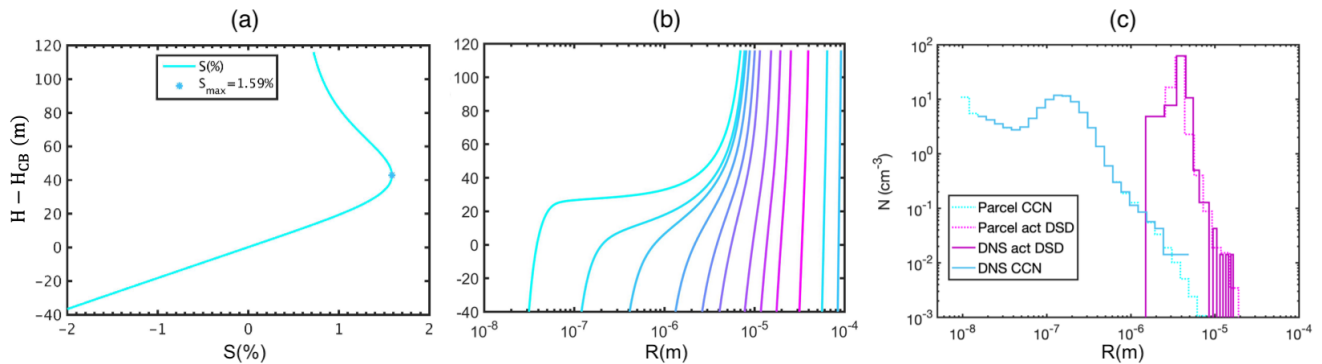


Figure 2. (a) Supersaturation and (b) radius of droplets with different initial wet sizes varying with the height from cloud base ($H - H_{CB}$). Only bins of activated particles are illustrated in (b). (c) The background natural CCN (dry particle) size distribution in the parcel model (light dotted blue histogram) and in the DNS model (darker solid blue histogram), and the droplet size distribution at maximum supersaturation ($S_{max} = 1.59\%$) in the parcel model (light dotted violet histogram) and in the DNS model (darker solid violet histogram).

parameter, κ , proposed by Petters and Kreidenweis (2007, their equation (6)) is employed in the droplet diffusional growth equation:

$$R \frac{dR}{dt} = \frac{S - \frac{R^3 - R_d^3}{R^3 - R_d^3(1 - \kappa)} \exp\left(\frac{2\sigma_w}{R_v \rho_w T R}\right)}{\frac{\rho_w R_v T}{e_s D'} + \frac{\rho_w L_v}{K' T} \left(\frac{1}{R_v T} - 1\right)} f_v, \quad (1)$$

105 here R is droplet radius, R_d is the radius of CCN, $\sigma_w = 7.2 \times 10^{-2} \text{ Jm}^{-2}$ is surface tension of water against air, $R_v = 467 \text{ Jkg}^{-1}\text{K}$ is individual gas constant for water vapor, ρ_w and ρ_a are the density of water and air, respectively, T is air temperature, and e_s is the saturated water vapor pressure. D' and K' are respectively the water vapor diffusivity and thermal conductivity that include kinetic effects (see equation (11a)-(11b) in Grabowski et al., 2011), and $L_v = 2.477 \times 10^6 \text{ Jkg}^{-1}$ is the latent heat of vaporization. S is supersaturation ratio defined as $\frac{q_v}{q_{vs}} - 1$ where q_v and q_{vs} are water vapor mixing ratios at the
 110 current condition and at saturated condition, respectively. f_v is ventilation coefficient which takes into account the distortion in water vapor field around the droplet surface when the droplet moves relative to the flow. Studies show that the effect is negligible when droplets are smaller than $10 \mu\text{m}$ in radius (Rogers and Yau, 1989, p116), and most droplets in the parcel model are below $10 \mu\text{m}$. Therefore, the ventilation effect is excluded in this phase, i.e., $f_v = 1$. In DNS, we apply the empirical formulas of f_v from Beard and Pruppacher (1971) which depends on the droplet Reynolds number and Schmidt number (see also equation
 115 (B2)-(B3) in Chen et al., 2018b).

There are two advantages of using the hygroscopicity parameter: 1) The chemical information of the aerosol (i.e., molecular weight, van Hoff factor, density, etc.) is simplified into a single parameter in the solute term; 2) the hygroscopicity parameter of mixed solute due to collision-coalescence can be simply calculated by a weighted average of the volume fractions of each component in the mixture (Petters and Kreidenweis, 2007).

120 The initial environmental conditions are taken from the cumulus cloud case of Jensen and Nugent (2017, Table 2). The parcel ascends from $H = 600 \text{ m}$ ($\approx 284 \text{ m}$ below cloud base) with a constant updraft velocity of 2.0 m s^{-1} , resembling a fair-weather cumulus cloud condition. The detailed information is listed in Table 1. The CCN (dry aerosol) size distribution fits a lognormal distribution, taken from the pristine case of Xue et al. (2010) (light blue histogram in Fig. 2(c)). The distribution consists of three log-normal modes in which the geometric mean dry radii in the three modes are $R = [0.0039, 0.133, 0.29] \mu\text{m}$, the
125 geometric standard deviations are $\sigma = [1.5128, 0.4835, 0.9118]$, and the total number concentrations of the whole size range are $N = [133, 66.6, 3.06] \text{ cm}^{-3}$. The initial size is discretized into 39 bins between $0.006 \mu\text{m}$ and $49 \mu\text{m}$, which gives a total number concentration $N = 112 \text{ cm}^{-3}$. It is worth noting that the number concentration of CCN larger than $10 \mu\text{m}$ is below 10^{-4} cm^{-3} , corresponding to less than one particle in the DNS domain ($L = 16.5 \text{ cm}$). The hygroscopicity parameter of all aerosols is assumed $\kappa = 0.47$. The moving-bin method or moving-size-grid method (see discussion in Yang et al., 2018)
130 is applied to calculate the evolution of the DSD. In this way, the numerical diffusion caused by the Eulerian bins can be avoided (Morrison et al., 2018; Grabowski et al., 2019). The initial wet size is the size when in equilibrium ($dR/dt = 0$) at the given ambient humidity (Jensen and Nugent, 2017). As illustrated in Fig. 2(b), the droplets with initial radius below $1 \mu\text{m}$ grow quickly by condensation between $20 - 40 \text{ m}$ above the cloud base before the maximum supersaturation is reached, and droplets larger than $1 \mu\text{m}$ grow slower, creating a narrow DSD near the cloud base.

Table 1. Model description and initial conditions of the parcel model and the DNS model.

	Parcel	DNS
Model description		
Domain size	0D air parcel	$0.165 \times 0.165 \times 0.165 \text{ m}^3$
Δx	-	$1.289 \times 10^{-3} \text{ m}$
Δt	10^{-4} s	$3.15 \times 10^{-5} \text{ s}$
Microphysics treatment	moving-bin method	Lagrangian particle method
Initial conditions		
Initial temperature	284.3 K	281.2 K
Initial pressure	938.5 hPa	902.2 hPa
Initial number concentration of natural background aerosols	112 cm^{-3}	85 cm^{-3}
Initial saturation ratio	85.61%	101.59%
Updraft velocity	2.0 m s^{-1}	2.0 m s^{-1}
Simulated time	300 sec	500 sec

135 2.2 DNS model

All DNS simulations are initialized with an identical mean state listed in Table 1. A constant mean updraft speed of 2 m s^{-1} is prescribed to lift the air parcel. The initial mean-state variables for DNS are obtained from the parcel model output at maximum supersaturation ($S = 1.59\%$). Above this altitude, no further activation is expected in the parcel due to the decreasing

140 supersaturation. The inactivated aerosols, corresponding to the first two bins of the light blue histogram in Fig. 2(c), do not influence the subsequent evolution of the DSD. Therefore, only the activated aerosols from the parcel model are carried over to the DNS, reducing the particle number concentration to $N = 85 \text{ cm}^{-3}$. This treatment avoids the computation of tracking the inactivated particles. In the parcel model, the droplet size is calculated by using the moving-bin method. The dry radius of each bin remains constant, and the wet radius grows by condensation. To assign the initial droplet size and its dry radius in the DNS, we regrouped the activated droplet bins into 15 droplet size groups ($R = 2 - 16 \mu\text{m}$) with an interval of $1 \mu\text{m}$. Their
145 CCN sizes remain the original value. Due to the parallelization setup in the model, the initial number of each droplet size group has to be an exact multiple of the number of processors in the simulation (64 processors are used in the present simulations). Therefore, a small difference in the resulting DSD between the two models is expected, as shown in Fig. 2(c).

The DNS model in the present study is initially developed by Vaillancourt et al. (2001) and has undergone a few modifications since then (Franklin et al., 2005; Chen et al., 2016, 2018a, b). The model employs two sets of equations: 1) the macroscopic
150 equations to calculate the base-state (parcel-mean) variables, and 2) the microscopic equations to calculate the fluctuation of the variables affected by the small-scale turbulence and the local droplet condensation. A detailed description of the DNS model can be found in Chen et al. (2018b, Section 2 and Appendix B).

Two modifications are made in the present study. First, we use equation (1) to replace the simplified version of the droplet growth equation in Chen et al. (2018b, equation (B1)) where the curvature term and the solute term are excluded. Parcel model
155 studies on droplet condensation in a lifted parcel show that the curvature term and the solute term can lead to condensational broadening on the droplet size spectrum. Srivastava (1991) demonstrated that the curvature effect is essential for DSD broadening in an ascending parcel. Korolev (1995) found that the curvature effect and the solute effect lead to irreversible broadening when supersaturation fluctuations are present. It is also found that aerosols of different sizes and different hygroscopicity can cause spectral broadening without supersaturation fluctuations (Çelik and Marwitz, 1999; Jensen and Nugent, 2017). There-
160 fore, it is crucial to examine whether these effects are important in spectral broadening when they dynamically couple with droplet collisional growth in a turbulent environment. Second, droplets with $R < 5 \mu\text{m}$ are treated as non-inertial particles due to their small Stokes number, i.e., their velocity is equal to the flow velocity. The length of a timestep is constrained by the inertial response time of the smallest inertial particle (see discussion in Chen et al., 2018a, on the length of the timestep). The treatment above avoids using too small a timestep when small aerosols are introduced. For droplets between $5 - 40 \mu\text{m}$,
165 their motion is determined by both the Stokes drag force and gravity, and for droplets over $40 \mu\text{m}$ nonlinear drag force is considered (see full description below the equation (B10) in Chen et al., 2018b). Droplets over $50 \mu\text{m}$ are treated as fall-out and are removed from the simulation.

2.3 DNS experimental design

Two sets of experiments are performed. Each set consists of six cases, which gives 12 simulations in total. The first set of
170 the experiments includes both condensational and collisional growth of droplets and will be referred to as the “condensation-collision” set. The second set excludes the droplet collision and will be referred to as the “condensation-only” set. The model setup for the two sets is the same other than the difference mentioned above. The configuration of the six cases is listed in Table

2. We focus on the condensation-collision set in the result section unless explicitly specified, and the condensation-only set is for the purpose of comparison to evaluate the influence by condensation and collision-coalescence.

Table 2. Model configuration of the six cases in each set of the experiment. Two sets of experiments are performed: set one includes both collision and condensation in the droplet growth and is referred to as the "condensation-collision" set; set two only considers droplet condensation and is referred to as the "condensation-only" set. This gives 12 cases in total. The natural DSD is taken from the parcel model output at $S = 1.59\%$. Monodisperse seeding is considered in "seeded" cases with CCN size (R_d) and initial droplet size (R) listed in the table.

Experiments		Turbulence	Solute effect	Initial DSD
Natural cases	Run A (CTL)	on	on	Natural DSD
	Run B (NoTurb)	off	on	Natural DSD
	Run C (NoSolu)	on	off	Natural DSD
"Seeded" cases	Run D1 (Seed-1N1R)	on	on	Natural DSD+ "seeding" aerosol ($R_d = 0.1 \mu m, R = 4 \mu m, N = 10 cm^{-3}$)
	Run D2 (Seed-2N1R)	on	on	Natural DSD + "seeding" aerosol ($R_d = 0.1 \mu m, R = 4 \mu m, N = 20 cm^{-3}$)
	Run D3 (Seed-1N2R)	on	on	Natural DSD + "seeding" aerosol ($R_d = 1 \mu m, R = 8 \mu m, N = 10 cm^{-3}$)

175 Run A (CTL) is the control run. Only one condition is changed in each of the other five cases. Runs A-C use the same initial DSD from the parcel model and are referred to as the "natural" cases. Turbulence and solute effect are switched off in Run B (NoTurb) and Run C (NoSolu), respectively, to gauge the effects of turbulence and CCN hygroscopicity on the DSD. When turbulence is switched off, the background velocity fluctuation is set to $0 m s^{-1}$. Therefore, particle motion is only affected by the mean updraft and gravitational settling, and the supersaturation fluctuation is only induced by droplet condensation and
180 evaporation. When the solute term is switched off, i.e., $\kappa = 0$, droplets consist of only pure water. Runs D1-D3 are referred to as "seeded" cases because an extra number of aerosols are introduced near the cloud base (at the beginning of DNS). Two seeding sizes and two number concentrations are considered, as described in Table 2. Different than the traditional cloud seeding, the same hygroscopicity of $\kappa = 0.47$ is assumed for both the natural aerosols and the seeding aerosols. In Run D1, we introduce seeding aerosol of dry radius $R_d = 0.1 \mu m$, wet radius $R = 4 \mu m$, and number concentration $N = 10 cm^{-3}$. We
185 double the seeding aerosol number concentration in Run D2 and increase tenfold the dry size in Run D3 (see Table 2). It should be pointed out that the dissipation rate in cumulus clouds tends to increase with height (Seifert et al., 2010). For simplicity, the eddy dissipation rate (ϵ) for all the turbulent cases is set statistically stationary ($\epsilon = 500 cm^2 s^{-3}$). The advantage of this idealized, simplified treatment is that the effect of turbulence can be easily separated from aerosol effects. A dissipation rate of $500 cm^2 s^{-3}$ represents a strongly turbulent environment in cumulus clouds to examine the upper-bound of turbulent effects
190 on the DSD evolution.

3 Results

3.1 Natural cases

We first compare the results of the natural cases (Run A-C) to examine the effect of turbulence and hygroscopicity (solute) on the droplet evolution. Fig. 3 shows that aerosol and turbulence effectively broaden the DSD at different times. Without
 195 hygroscopic aerosols in Run C (NoSolu), the DSD broadening is suppressed within the first six minutes. However, the tail evolution quickly catches up and converges to that in Run A (CTL) afterwards. Meanwhile, switching off turbulence in Run B (NoTurb) suppresses the DSD broadening at a later time (Fig. 3). The tail of the spectrum in Run A and Run B stays similar in the first two minutes and starts to differ by a large amount afterwards.

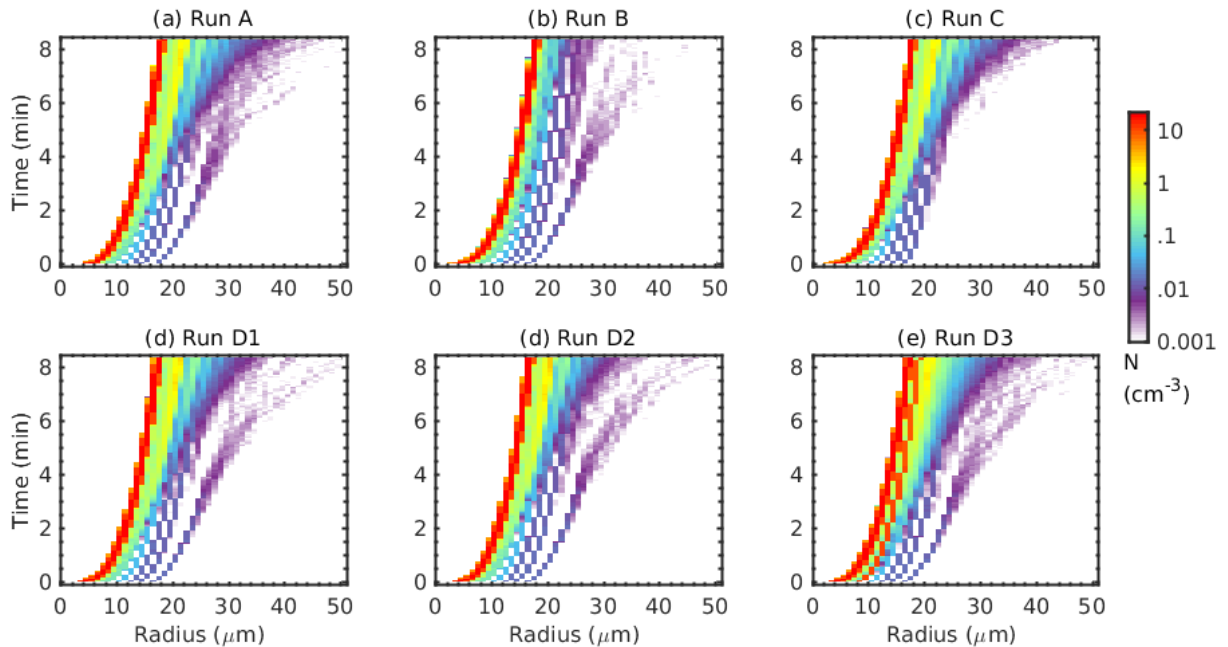


Figure 3. Time evolution of the droplet size distribution in the condensation-collision set of experiments. The droplet number concentration (cm^{-3}) is indicated by colors with its value shown in the color bar. The configuration of each experiment is listed in Table 2.

Turbulence effects on the DSD broadening is minor before $T=6$ min (Fig. 4(a-b)). Both Run A and Run B produce a similar
 200 number of droplets over $25 \mu m$ at $T=6$ min. The majority of this size group is grown from the ultra giant aerosol with an initial dry and wet size of $R_d = 4.9 \mu m$ and $R = 16 \mu m$. They grow rapidly to $25 \mu m$ by condensation within the first two minutes in both Run A and B. However, droplets can hardly reach beyond $30 \mu m$ solely by condensation (Fig. 4 (d-e)). The tail over $30 \mu m$ is mainly formed by the subsequent collision-coalescence process. Once droplets are over $25 \mu m$, the gravitational collection becomes effective, leading to a similar DSD tail with or without turbulence. However, gravitational collection of
 205 droplets below $25 \mu m$ in Run B is ineffective to sustain the formation of large droplets. After $T=6$ min, the tail of DSD in

Run B becomes quasi-stationary for droplets over $20 \mu m$ (red and blue histograms in Fig. 4(b)) due to negligible gravitational collisions. This can be illustrated by a negligible collision frequency in Run B in Fig. 6(e). In contrast, a substantial number of droplets $> 20 \mu m$ are constantly formed in Run A after $T=2$ min through rapid turbulent collisions. Comparing to collision frequency in Run B (Fig. 5 (b)), turbulence substantially enhances the collisional growth of droplets of $R < 20 \mu m$. The total collisions in turbulent cases increase by a factor of 20. It is also found that the turbulent enhancement of collisions is strongest among droplet pairs of similar sizes, i.e., with a radius ratio of $r/R > 0.8$. Similar-sized collisions increase by nearly a factor of 50 in turbulent cases, contributing to over 80% of the total collisions as opposed to 34% in Run B. This is because a non-turbulent environment does not favor similar-sized collisions due to a similar droplet settling speed. Turbulence, on the one hand, increases the relative motion between droplets and on the other hand, induces a stronger clustering of similar-sized droplets. The two effects jointly strengthen the similar-sized collisions. The turbulent enhancement on similar-sized collisions is then amplified by the condensational process. Chen et al. (2018b) also demonstrated that as the condensation process reduces the DSD width and generates more similar-sized droplets, turbulence enhances the similar-sized collision and thus broadens the DSD.

Even though turbulence intensifies the collisional growth, the modulation on the droplet condensation is found insignificant. The DSDs in Run A and B in the condensation-only set are nearly identical (Fig. 4 (d-e)). This is because the supersaturation fluctuations are weak in an adiabatic core region. Vaillancourt et al. (2002) found that in a quasi-adiabatic environment both particle sedimentation and short-lived turbulent coherent structure reduce the supersaturation fluctuation and decrease the time that droplets are exposed to these fluctuations. We expect that the turbulent-induced condensational broadening is more significant in the cloud edge where entrainment mixing induces large variation in supersaturation fluctuations.

When solute effect is removed in Run C (NoSolu), droplets can hardly reach beyond $30 \mu m$ before $T=6$ minute (Fig. 4 (c)) because of a lack of ultra-giant aerosols ($R_d > 4 \mu m$). Embryonic drizzle drops at the early-stage ($T < 6$ min) are formed from the fast growth of the ultra-giant aerosols as seen in both Run A and Run B. No significant change is found in the mean droplet radius and the relative dispersion between Run A and Run C (Fig. 7(d)). Only a slightly lower collision frequency in the droplet size group of $R > 20 \mu m$ results from a lack of ultra-giant aerosols (see the green histograms in Fig. 5). This implies that the solute effect on droplet condensation in DSD broadening is small for aerosols below $R_d < 4 \mu m$. The ultra giant aerosols ($R_d = 4.9 \mu m$ in this study), due to their scarcity, have a negligible contribution in shifting the mean radius and relative dispersion (Fig. 7). As shown in Fig. 3(c), an efficient broadening is triggered at $T = 6$ minute, resulting in a similar DSD as in Run A at the end of the simulation. It is shown that droplets between $20 - 30 \mu m$ are produced through turbulent collisions by the end of $T = 6$ minutes (Fig. 4(c)), causing a boost in collisions of droplets over $20 \mu m$ (Fig. 6(d)).

The time evolution of collision frequency in Fig. 6 shows that all five turbulent cases show a similar trend in total collisional frequency, even though the trend at the four size groups varies. The gravitational collection process is very weak with the collision frequency lowered by at least one order of magnitude in Run B. Still, a slightly higher droplet number concentration at $R > 40 \mu m$ is observed in both Run A and B than in Run C, because of the presence of ultra giant aerosols. At the same time, the collision frequency of the four size groups in Run A and Run C are almost identical. Even though the ultra giant

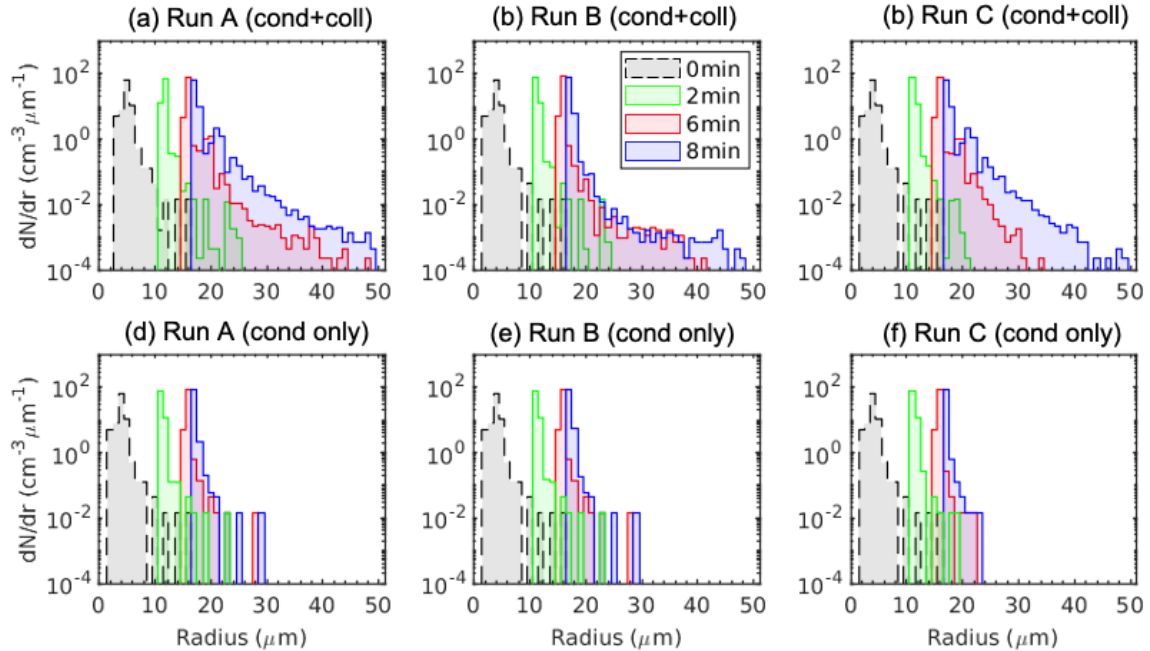


Figure 4. Droplet size distributions (DSDs) at $T = 0 \text{ min}$ (grey), $T = 2 \text{ min}$ (green), $T = 6 \text{ min}$ (red), and $T = 8 \text{ min}$ (blue) of the natural cases (Run A-C). The upper panel (a-c) is the DSD in the condensation-collision set of experiments, and the lower panel (d-e) is the DSD in the condensation-only set of experiments.

240 aerosols are important in forming early drizzle embryos, due to a low number concentration, they do not sustain an efficient collectional process.

The relative dispersion, defined as the ratio between the standard deviation of the DSD and the mean droplet radius, is an indicator of the width of the DSD. Condensational growth narrows the DSD and decreases the relative dispersion in the condensation-only set (dotted lines in Fig. 7 (c)). Droplet growth in the first two minutes is prevailed by condensation, as the relative dispersion in the condensation-collision set of experiments well overlaps with that in the condensation-only set. After $T = 2 \text{ min}$ the relative dispersion in the condensation-collision set and the condensation-only set starts to deviate from one another. This is mainly due to two factors: 1) the condensation narrowing slows down as droplets get larger and supersaturation gets lower; 2) the collision rate increases with the increasing droplet mean radius and thus leads to a higher collision rate to strengthen the DSD broadening. In Run B, the collision rate stays the lowest of all cases throughout the simulation (Fig. 6 (e)), leading to the smallest relative dispersion of all the six cases.

250 It is recognized that the relative dispersion of around 0.1 in this study is smaller than observed in most flight measurements. Firstly, the flight measurement is an average of a long-distance sampling ($\mathcal{O}(100m)$) which does not capture the local property of droplet size distribution and therefore is not comparable to our modeled results. Secondly, the simulations only last for 500s,

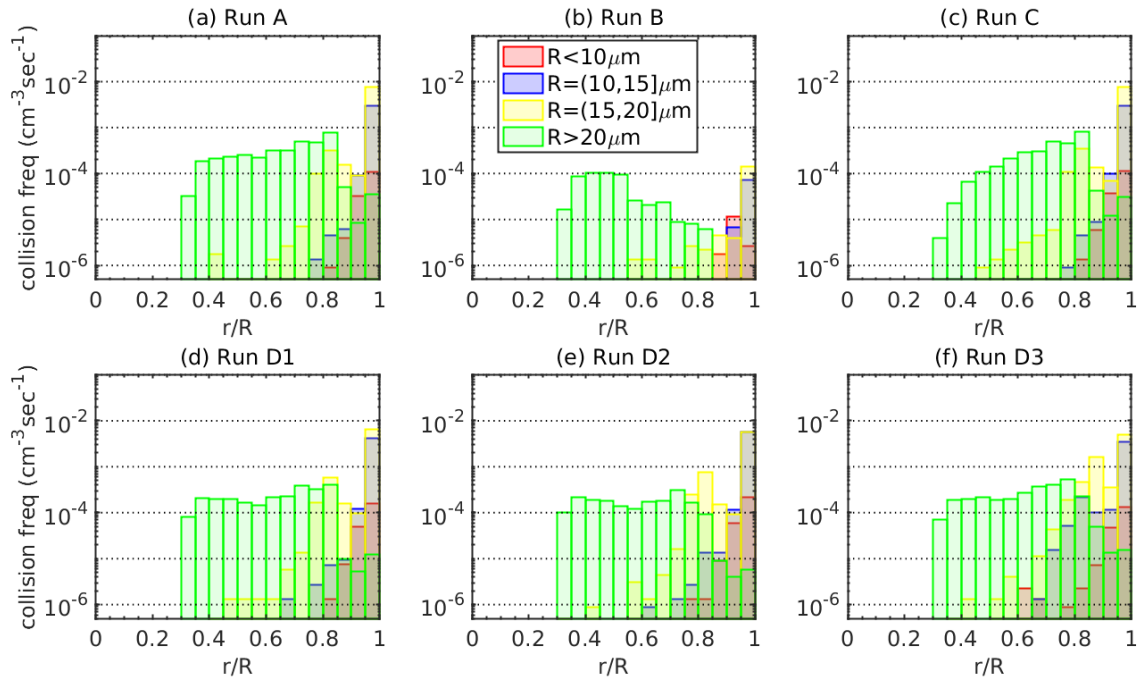


Figure 5. Collision frequency varying with r/R in the condensation-collision set of experiments. r/R is the radius ratio between the small droplet and the large droplet of collided droplet pairs. The droplet pairs are divided into four size groups by the big droplet radius, R , shown in the legend.

and it is expected that the relative dispersion keeps growing. Thirdly, our idealized simulation focuses on the cloud adiabatic
 255 core which is devoid of entrainment. Inhomogeneous mixing by entrainment can possibly broaden the DSD.

Despite that DSDs differ among the six cases, the modulation of the bulk condensation by both turbulence and aerosol is negligible, as supported by an almost identical LWC of the six cases (Fig. 7(a)). Turbulence and aerosols redistribute water mass among different droplet sizes by modifying the condensational and collisional growth of individual droplets, thus shifting the droplet statistics such as the mean radius and relative dispersion, and eventually alters the autoconversion rate (Fig. 7(f)).
 260 It is also found that even though Run B produces the second largest mean radius, the autoconversion rate stays the lowest, accompanied by the smallest relative-dispersion. Therefore, properties such as the shape of the DSD and relative dispersion are more relevant to autoconversion than the LWC. The traditional autoconversion parameterizations such as the Kessler-type parameterization (Kessler, 1969; Liu and Daum, 2004) and the Sundqvist-type parameterizations (Sundqvist, 1978; Liu et al., 2006) customarily use a threshold function based on the mean radius and/or the LWC. It is suggested that autoconversion rate
 265 is also influenced by various other parameters (see Noh et al., 2018, and references therein). The present study demonstrates that both parameters, in particular, the LWC cannot properly capture the trend of the autoconversion. The autoconversion rate by Berry and Reinhardt (1974), and its modified versions which include both the mean droplet size and dispersion parameter,

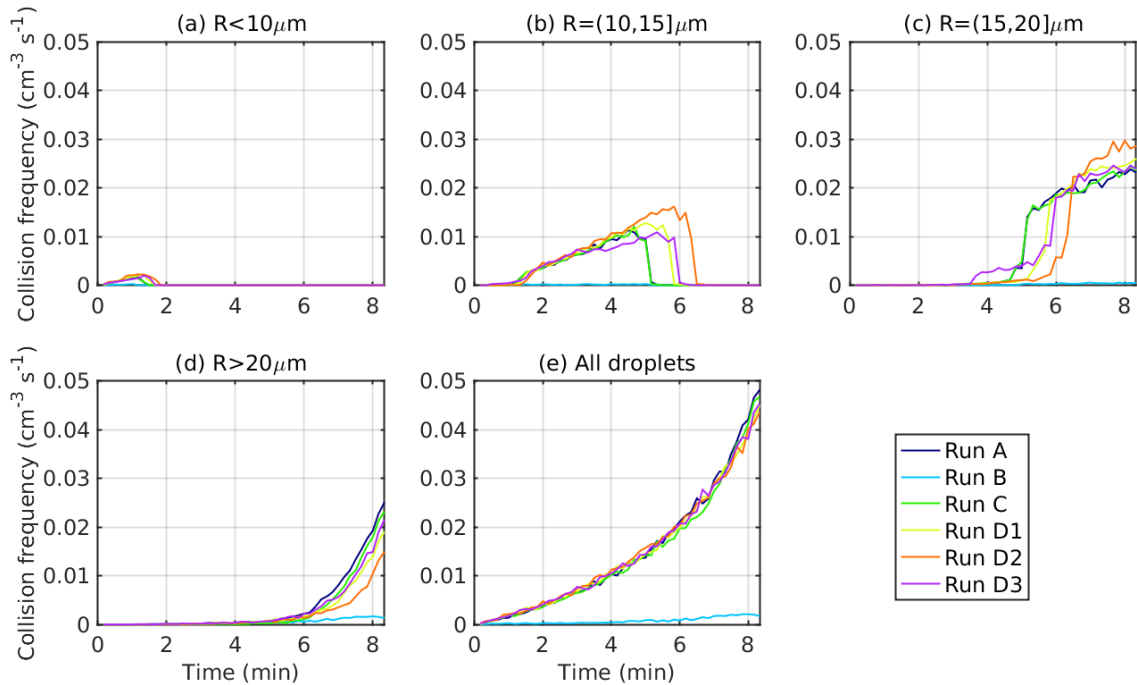


Figure 6. (a-d) Time evolution of collision frequency for droplet pairs of four different size groups mentioned in Fig. 5. (e) Time evolution of collision frequency for all droplet pairs.

is conceptually better than the Kessler-type schemes. Our results thus agree with Gilmore and Straka (2008) which found that the scheme of Berry and Reinhardt (1974) is more sophisticated and requires less tuning to match the observed onset of rain and proportions of cloud and rain. They also found that the growth rate of rain mass and number concentration are highly sensitive to the shape and dispersion parameters. Additionally, it is worth noting that turbulence modifies the collision rate and thus shifts the DSD shape and relative dispersion. Therefore, a turbulence-dependent relative-dispersion parameter is needed in developing the autoconversion scheme.

3.2 Seeded cases

Seeding reduces the mean droplet radius due to higher competition for water vapor among individual droplets (Fig. 7 (d)). Therefore seeding slows down the autoconversion process. Nevertheless, the LWC is not affected by seeding (Fig. 7(a)), which again indicates that the LWC is not a well-related quantity to autoconversion in this case.

When investigating the relative importance of aerosol and turbulence to droplet growth, it is found that the modulation of droplet mean radius by aerosols is larger than the modulation by collision-coalescence. In Fig. 7 (d), the difference between seeded and unseeded cases exceeds the difference between the condensation-only set (dotted lines) and condensation-collision set (solid lines) of each case. Regardless, turbulent collision-coalescence yields large droplets over $30 \mu m$ and increases the

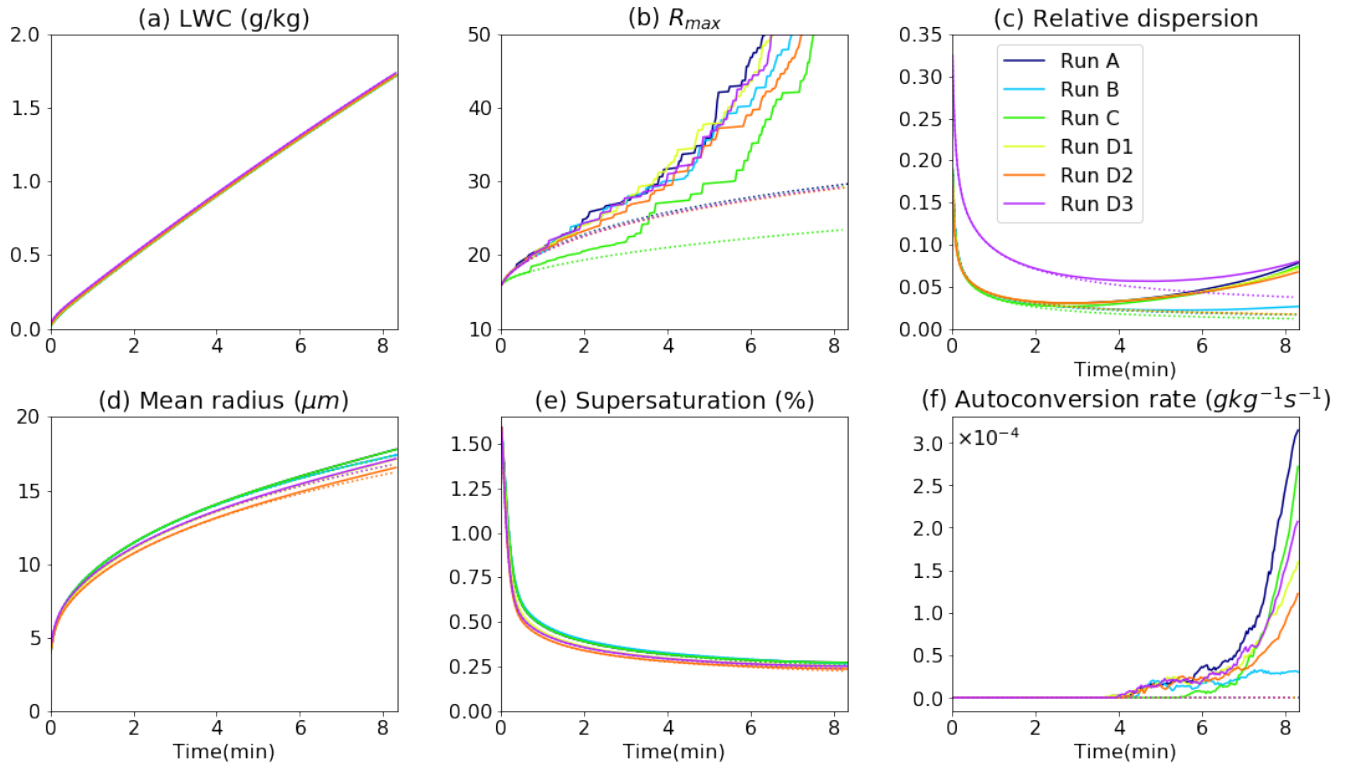


Figure 7. The temporal variation of parcel-mean (a) liquid water content (LWC), (b) maximum droplet radius (R_{max}), (c) relative dispersion, (d) droplet mean radius, (e) supersaturation ratio, and (f) autoconversion rate in the condensation-collision set of experiments (solid lines) and in the condensation-only set of experiments (dotted lines). The relative dispersion is defined as the standard deviation of the droplet radius divided by the mean radius. The autoconversion rate here is defined as the mass transfer rate from droplet smaller than $R = 30 \mu m$ to droplet larger than $30 \mu m$. The droplets over $50 \mu m$ are treated as fall-outs and removed from the domain. Thus (b) only shows a maximum droplet size at $50 \mu m$.

width of the DSD. The total collision rate is heavily determined by the turbulence level and mildly affected by seeding or CCN hygroscopicity (Fig. 6(e)). Besides, the change in R_{max} and relative dispersion due to collisions exceeds that from changing the aerosol condition. As condensational growth can hardly produce droplets over $30 \mu m$, turbulent enhancement of collision is determinant in the mass conversion from small droplets to drizzle embryos. Meanwhile, seeding increases the competition for water vapor among droplets and reduces the mean droplet size, leading to more collisions of small droplets and fewer collisions of large droplets (Fig. 6(a-d)). Specifically, by doubling the seeding aerosol number in Run D2 (Seed-2N1R), the condensational growth of small droplets is further prohibited due to a higher competition of water vapor, resulting in more small droplets. Increasing the size of seeding aerosols in Run D3 (Seed-1N2R) buffers the inhibition effect. The resulting autoconversion rate is Run A > Run D3 > Run D1 > Run D2.

Finally, aerosol hygroscopicity is key to the onset time of autoconversion. All five aerosol-embedded cases see a similar onset time around $T = 4$ min. Removing the solute effect (hygroscopic material) in Run C delays the onset of autoconversion by about 1.5 min (green line Fig. 7 (f)). Nevertheless, after $T = 6-7$ min, the autoconversion rate in Run C exceeds all seeded cases. First, solute (CCN hygroscopicity) has a negligible effect on the growth of small aerosols, as the size distribution of small droplets in Run A and C remain almost identical. This is substantiated by the almost identical collision frequency of droplets below $20 \mu m$ of the two cases (Fig. 6 (a-c)). Second, seeding reduces the mean radius of the droplets. This leads to a reduction in collisions for droplets over $20 \mu m$ (Fig. 6(d)) and subsequently decelerates the autoconversion process. The above findings imply that increasing the aerosol size (ultra-giant aerosol) shortens the lifetime of the clouds through a fast onset of rain. And increasing the number of aerosols decelerates the rain process.

300 4 Summary and discussion

This paper investigates the effects of turbulence and aerosol properties (hygroscopicity, number concentration, and size) on the microphysics during early cloud and rain development. A parcel-DNS hybrid modeling framework is developed. The parcel model is used to generate the initial size distribution of activated aerosols, and the DNS model calculates the subsequent growth of those activated aerosols affected by both the microscopic (turbulent fluctuation) and the macroscopic (parcel mean) environment. By using this economical modeling framework, continuous particle growth from sub-cloud aerosols to cloud droplets is accurately represented.

Overall, ultra-giant aerosols in the natural cases quickly form the drizzle embryo and thus determine the onset time of autoconversion. However, they only form a few big raindrops due to their scarcity, which has little impact on the level of autoconversion. Turbulence enhances the collision frequency by more than one order of magnitude and determines the level of autoconversion. Specifically, turbulence enhances the collisions among similar-sized droplets that are less likely to happen in a non-turbulent environment, effectively broadening the DSD. Therefore, the autoconversion in a turbulent environment is significantly greater than in a non-turbulent environment. It is also found that seeding (increasing aerosol number and size) modifies the level of autoconversion. On the one hand, increasing the aerosol number reduces the mean radius due to stronger competition for water vapor, and therefore slows down the autoconversion. On the other hand, increasing the seeding size can buffer such negative feedback. However, the seeding particles in this study only cover a limited range of dry radius ($R = 0.1, 1 \mu m$) and number concentration ($N = 10, 20 cm^{-3}$, corresponding to 10 – 20% increase in the total number concentration). Conditions with more ultra-giant aerosols ($R \gg 1 \mu m$), lower aerosol concentrations ($N \ll 100 cm^{-3}$), or highly polluted environment ($N \gg 100 cm^{-3}$) will be of interest to further assess the relative importance of aerosols and turbulence. It is argued that predicting the rain onset time requires accurate information and representation of ultra-giant aerosols. And an accurate autoconversion scheme requires a well-quantified turbulent collisions kernel.

Even though the autoconversion rate differs among the six cases, it is found that the parcel-mean variables such as LWC, mean radius, and supersaturation are not sensitive to turbulence level and aerosol conditions. In this case the LWC and mean droplet radius, which are key parameters in Kessler-type or Sundqvist-type autoconversion parameterizations, are not well-

related quantities to autoconversion rate, and information of turbulence intensity and aerosols are essential to determine the
325 autoconversion rate. It is argued that these parcel-mean variables are mainly affected by the updraft speed which is held the
same among the six cases. Sensitivity studies are needed in the future to investigate the effect of the LWC on the autoconversion
rate due to a change in the updraft.

Cloud models are sensitive to microphysics schemes, and the autoconversion parameterization is one of the main sources
of uncertainty in the representation of warm clouds and rain with few observations to verify against. The large uncertainty
330 may be ascribed to the decoupling of microphysics from subgrid-scale turbulence and a lack of aerosol information in the
parameterization. Therefore, the aerosol effect evaluated by the models should be cautiously interpreted. The hybrid parcel-
DNS model can be used for verifying the autoconversion rate affected by turbulence and aerosols at the sub-grid scale of
large-eddy simulation (LES).

Despite a good number of improvements made, the current modeling framework still presents the following shortcomings:
335 for simplicity, the same hygroscopic parameter ($\kappa = 0.47$) is assumed among the natural aerosols and the seeding aerosols.
Besides, seeding is initialized 40 m above the cloud base while traditional hygroscopic seeding introduces particles around
100 – 300 m below the cloud base. This treatment might affect the model results as seeding below the cloud base influences
the activation and growth of the background aerosols and thus modifies the DSD at the cloud base (Cooper et al., 1997).

Our idealized simulations focus on the cloud adiabatic core region and therefore exclude entrainment mixing which is
340 highly active near the cloud edge. The activation of newly entrained aerosols might lead to a further broadening of the DSD
(e.g., Lasher-Trapp et al., 2005). In addition, the in-cloud mixing at a much larger scale than the DNS domain transports
and mixes both the air and droplets from different parts of the cloud including the cloud edge, leading to a highly perturbed
Lagrangian supersaturation experienced by droplets (Grabowski and Abade, 2017, "eddy hopping effect"). On the other hand,
larger turbulent eddies can generate higher supersaturation fluctuations due to a higher variation in a vertical motion and thus
345 may both affect the aerosol activation and broaden the DSD. Traditional DNS which is confined to a relatively small domain
size (<1 m), and the impact of supersaturation fluctuations is significantly restricted. Methods such as an up-scaled DNS with
superdroplets (e.g., Thomas et al., 2020) or representing the large-scale mixing with an external forcing on the thermodynamic
fields (Paoli and Shariff, 2009) can be used for studying the impact of turbulent scales on the supersaturation fluctuations and
thus on the condensational broadening of DSD. In conclusion, the relative importance of entrainment, eddy hopping effect,
350 small-scale turbulence and aerosols requires further investigation.

This study proposes the first DNS model framework for scrutinizing the microphysical impact of cloud seeding and presents
the first results of such a model. Full DNS modeling from below the cloud base will be the next step to include the effect of
turbulence on aerosol activation. Additionally, more realistic scenarios resembling actual hygroscopic seeding conditions, such
as utilizing multi-disperse size distributions, different hygroscopicity parameters, and seeding below the cloud base will be
355 designed in the future development and deployment of this framework.

Code and data availability. The data produced by the Direct Numerical Simulation (DNS) model and parcel model can be accessed in the Harvard Dataverse repository (Chen et al., 2019, doi:10.7910/DVN/HBIKKV). The parcel model and DNS model used to produce the dataset are available upon request.

360 *Author contributions.* This study was co-designed by Sisi Chen, Lulin Xue, and M.K. Yau. Sisi Chen conducted the model simulation, did the data analysis, and wrote the manuscript. Lulin Xue and M.K. Yau provided advice and discussions on the model results and revised the manuscript.

Competing interests. The authors declare that they have no conflict of interest.

365 *Acknowledgements.* We thank the two anonymous reviewers for their invaluable comments. This work is supported by the National Center for Atmospheric Research, sponsored by the National Science Foundation under Cooperative Agreement No. 1852977. Part of this work is supported by the National Center of Meteorology, Abu Dhabi, UAE under the UAE Research Program for Rain Enhancement Science. We would like to acknowledge high-performance computing (HPC) support from Cheyenne, Graham, and Cedar. HPC resources at Cheyenne (doi:10.5065/D6RX99HX) is provided by NCAR's Computational and Information Systems Laboratory and sponsored by the National Science Foundation. HPC resources at Graham and Cedar are provided by Compute Canada (www.computecanada.ca).

References

- 370 Beard, K. V. and Pruppacher, H. R.: A Wind Tunnel Investigation of the Rate of Evaporation of Small Water Drops Falling at Terminal Velocity in Air, *J. Atmos. Sci.*, 28, 1455–1464, [https://doi.org/10.1175/1520-0469\(1971\)028<1455:awtiot>2.0.co;2](https://doi.org/10.1175/1520-0469(1971)028<1455:awtiot>2.0.co;2), 1971.
- Berry, E. X. and Reinhardt, R. L.: An Analysis of Cloud Drop Growth by Collection Part II. Single Initial Distributions, *J. Atmos. Sci.*, 31, 1825–1831, [https://doi.org/10.1175/1520-0469\(1974\)031<1825:aaocdg>2.0.co;2](https://doi.org/10.1175/1520-0469(1974)031<1825:aaocdg>2.0.co;2), 1974.
- Çelik, F. and Marwitz, J. D.: Droplet Spectra Broadening by Ripening Process. Part I: Roles of Curvature and Salinity of Cloud Droplets, *Journal of the Atmospheric Sciences*, 56, 3091–3105, [https://doi.org/10.1175/1520-0469\(1999\)056<3091:dsbbrp>2.0.co;2](https://doi.org/10.1175/1520-0469(1999)056<3091:dsbbrp>2.0.co;2), 1999.
- 375 Chen, S., Bartello, P., Yau, M. K., Vaillancourt, P. A., and Zwijssen, K.: Cloud Droplet Collisions in Turbulent Environment: Collision Statistics and Parameterization, *J. Atmos. Sci.*, 73, 621–636, <https://doi.org/10.1175/JAS-D-15-0203.1>, 2016.
- Chen, S., Yau, M. K., and Bartello, P.: Turbulence Effects of Collision Efficiency and Broadening of Droplet Size Distribution in Cumulus Clouds, *J. Atmos. Sci.*, 75, 203–217, <https://doi.org/10.1175/JAS-D-17-0123.1>, 2018a.
- 380 Chen, S., Yau, M.-K., Bartello, P., and Xue, L.: Bridging the condensation–collision size gap: a direct numerical simulation of continuous droplet growth in turbulent clouds, *Atmos. Chem. Phys.*, 18, 7251–7262, <https://doi.org/10.5194/acp-18-7251-2018>, 2018b.
- Chen, S., Xue, L., and Yau, M.: Data support for “Impact of CCN hygroscopicity and turbulence on cloud droplet growth: An in-cloud seeding case study using parcel-DNS approach”, <https://doi.org/10.7910/DVN/HBIKKV>, <https://doi.org/10.7910/DVN/HBIKKV>, 2019.
- Cooper, W. A., Bruintjes, R. T., and Mather, G. K.: Calculations Pertaining to Hygroscopic Seeding with Flares, *J. Appl Meteorol.*, 36, 1449–1469, [https://doi.org/10.1175/1520-0450\(1997\)036<1449:cpthsw>2.0.co;2](https://doi.org/10.1175/1520-0450(1997)036<1449:cpthsw>2.0.co;2), 1997.
- 385 Fan, J., Wang, Y., Rosenfeld, D., and Liu, X.: Review of Aerosol–Cloud Interactions: Mechanisms, Significance, and Challenges, *J. Atmos. Sci.*, 73, 4221–4252, <https://doi.org/10.1175/JAS-D-16-0037.1>, 2016.
- Franklin, C. N., Vaillancourt, P. A., Yau, M. K., and Bartello, P.: Collision Rates of Cloud Droplets in Turbulent Flow, *J. Atmos. Sci.*, 62, 2451–2466, <https://doi.org/10.1175/jas3493.1>, 2005.
- 390 Gilmore, M. S. and Straka, J. M.: The Berry and Reinhardt Autoconversion Parameterization: A Digest, *J. Appl. Meteorol. Clim.*, 47, 375–396, <https://doi.org/10.1175/2007jame1573.1>, 2008.
- Gotoh, T., Suehiro, T., and Saito, I.: Continuous growth of cloud droplets in cumulus cloud, *New Journal of Physics*, 18, 043 042, <https://doi.org/10.1088/1367-2630/18/4/043042>, 2016.
- Grabowski, W. W. and Abade, G. C.: Broadening of Cloud Droplet Spectra through Eddy Hopping: Turbulent Adiabatic Parcel Simulations, *Journal of the Atmospheric Sciences*, 74, 1485–1493, <https://doi.org/10.1175/jas-d-17-0043.1>, 2017.
- 395 Grabowski, W. W., Andrejczuk, M., and Wang, L.-P.: Droplet growth in a bin warm-rain scheme with Twomey CCN activation, *Atmos. Res.*, 99, 290–301, <https://doi.org/10.1016/j.atmosres.2010.10.020>, 2011.
- Grabowski, W. W., Morrison, H., Shima, S.-I., Abade, G. C., Dziekan, P., and Pawlowska, H.: Modeling of Cloud Microphysics: Can We Do Better?, *B. Am. Meteorol. Soc.*, 100, 655–672, <https://doi.org/10.1175/BAMS-D-18-0005.1>, 2019.
- 400 Jensen, J. B. and Nugent, A. D.: Condensational Growth of Drops Formed on Giant Sea-Salt Aerosol Particles, *J. Atmos. Sci.*, 74, 679–697, <https://doi.org/10.1175/jas-d-15-0370.1>, 2017.
- Kessler, E.: On the Distribution and Continuity of Water Substance in Atmospheric Circulations, in: *On the Distribution and Continuity of Water Substance in Atmospheric Circulations*, pp. 1–84, American Meteorological Society, https://doi.org/10.1007/978-1-935704-36-2_1, 1969.

- 405 Khain, A., Prabha, T. V., Benmoshe, N., Pandithurai, G., and Ovchinnikov, M.: The mechanism of first raindrops formation in deep convective clouds, *Journal of Geophysical Research: Atmospheres*, 118, 9123–9140, <https://doi.org/10.1002/jgrd.50641>, 2013.
- Korolev, A. V.: The Influence of Supersaturation Fluctuations on Droplet Size Spectra Formation, *Journal of the Atmospheric Sciences*, 52, 3620–3634, [https://doi.org/10.1175/1520-0469\(1995\)052<3620:tiosfo>2.0.co;2](https://doi.org/10.1175/1520-0469(1995)052<3620:tiosfo>2.0.co;2), 1995.
- Lasher-Trapp, S. G., Cooper, W. A., and Blyth, A. M.: Broadening of droplet size distributions from entrainment and mixing in a cumulus
410 cloud, *Quarterly Journal of the Royal Meteorological Society*, 131, 195–220, <https://doi.org/10.1256/qj.03.199>, 2005.
- Li, X.-Y., Brandenburg, A., Svensson, G., Haugen, N. E. L., Mehlig, B., and Rogachevskii, I.: Condensational and Collisional Growth of Cloud Droplets in a Turbulent Environment, *Journal of the Atmospheric Sciences*, 77, 337–353, <https://doi.org/10.1175/jas-d-19-0107.1>, 2020.
- Liu, Y. and Daum, P. H.: Parameterization of the Autoconversion Process. Part I: Analytical Formulation of the Kessler-Type Parameteriza-
415 tions, *J. Atmos. Sci.*, 61, 1539–1548, [https://doi.org/10.1175/1520-0469\(2004\)061<1539:potapi>2.0.co;2](https://doi.org/10.1175/1520-0469(2004)061<1539:potapi>2.0.co;2), 2004.
- Liu, Y., Daum, P. H., McGraw, R., and Wood, R.: Parameterization of the Autoconversion Process. Part II: Generalization of Sundqvist-Type Parameterizations, *J. Atmos. Sci.*, 63, 1103–1109, <https://doi.org/10.1175/jas3675.1>, 2006.
- Morrison, H., Witte, M., Bryan, G. H., Harrington, J. Y., and Lebo, Z. J.: Broadening of Modeled Cloud Droplet Spectra Using Bin Micro- physics in an Eulerian Spatial Domain, *J. Atmos. Sci.*, 75, 4005–4030, <https://doi.org/10.1175/jas-d-18-0055.1>, 2018.
- 420 Noh, Y., Oh, D., Hoffmann, F., and Raasch, S.: A Cloud Microphysics Parameterization for Shallow Cumulus Clouds Based on Lagrangian Cloud Model Simulations, *Journal of the Atmospheric Sciences*, 75, 4031–4047, <https://doi.org/10.1175/jas-d-18-0080.1>, 2018.
- Paoli, R. and Shariff, K.: Turbulent Condensation of Droplets: Direct Simulation and a Stochastic Model, *J. Atmos. Sci.*, 66, 723–740, <https://doi.org/10.1175/2008JAS2734.1>, 2009.
- Petters, M. D. and Kreidenweis, S. M.: A single parameter representation of hygroscopic growth and cloud condensation nucleus activity,
425 *Atmos. Chem. Phys.*, 7, 1961–1971, <https://doi.org/10.5194/acp-7-1961-2007>, 2007.
- Rogers, R. R. and Yau, M. K.: *A Short Course in Cloud Physics*, Butterworth-Heinemann, 3rd edn., 1989.
- Saito, I. and Gotoh, T.: Turbulence and cloud droplets in cumulus clouds, *New Journal of Physics*, 20, 023 001, <https://doi.org/10.1088/1367-2630/aaa229>, 2018.
- Sardina, G., Picano, F., Brandt, L., and Caballero, R.: Continuous Growth of Droplet Size Variance due to Condensation in Turbulent Clouds,
430 *Phys. Rev. Lett.*, 115, 184 501, <https://doi.org/10.1103/PhysRevLett.115.184501>, 2015.
- Seifert, A., Nuijens, L., and Stevens, B.: Turbulence effects on warm-rain autoconversion in precipitating shallow convection, *Quarterly Journal of the Royal Meteorological Society*, 136, 1753–1762, <https://doi.org/10.1002/qj.684>, 2010.
- Srivastava, R. C.: Growth of Cloud Drops by Condensation: Effect of Surface Tension on the Dispersion of Drop Sizes, *Journal of the Atmospheric Sciences*, 48, 1596–1599, [https://doi.org/10.1175/1520-0469\(1991\)048<1596:gocdbc>2.0.co;2](https://doi.org/10.1175/1520-0469(1991)048<1596:gocdbc>2.0.co;2), 1991.
- 435 Stoelinga, M. T., Hobbs, P. V., Mass, C. F., Locatelli, J. D., Colle, B. A., Houze, R. A., Rangno, A. L., Bond, N. A., Smull, B. F., Rasmussen, R. M., Thompson, G., and Colman, B. R.: Improvement of Microphysical Parameterization through Observational Verification Experiment, *B. Am. Meteorol. Soc.*, 84, 1807–1826, <https://doi.org/10.1175/BAMS-84-12-1807>, 2003.
- Sundqvist, H.: A parameterization scheme for non-convective condensation including prediction of cloud water content, *Q. J. Roy. Meteor. Soc.*, 104, 677–690, <https://doi.org/10.1002/qj.49710444110>, 1978.
- 440 Thomas, L., Grabowski, W. W., and Kumar, B.: Diffusional growth of cloud droplets in homogeneous isotropic turbulence: DNS, scaled-up DNS, and stochastic model, *Atmospheric Chemistry and Physics Discussions*, 2020, 1–21, <https://doi.org/10.5194/acp-2020-159>, <https://www.atmos-chem-phys-discuss.net/acp-2020-159/>, 2020.

- Thomas, S., Ovchinnikov, M., Yang, F., Voort, D., Cantrell, W., Krueger, S. K., and Shaw, R. A.: Scaling of an Atmospheric Model to Simulate Turbulence and Cloud Microphysics in the Pi Chamber, *J. Adv. Model Earth Sy.*, 11, 1981–1994, <https://doi.org/10.1029/2019ms001670>, 2019.
- 445 Vaillancourt, P. A., Yau, M. K., and Grabowski, W. W.: Microscopic Approach to Cloud Droplet Growth by Condensation. Part I: Model Description and Results without Turbulence, *J. Atmos. Sci.*, 58, 1945–1964, [https://doi.org/10.1175/1520-0469\(2001\)058<1945:MATCDG>2.0.CO;2](https://doi.org/10.1175/1520-0469(2001)058<1945:MATCDG>2.0.CO;2), 2001.
- Vaillancourt, P. A., Yau, M. K., Bartello, P., and Grabowski, W. W.: Microscopic Approach to Cloud Droplet Growth by Condensation. Part II: Turbulence, Clustering, and Condensational Growth, *J. Atmos. Sci.*, 59, 3421–3435, [https://doi.org/10.1175/1520-0469\(2002\)059<3421:MATCDG>2.0.CO;2](https://doi.org/10.1175/1520-0469(2002)059<3421:MATCDG>2.0.CO;2), 2002.
- 450 Wang, L.-P., Ayala, O., Kasprzak, S. E., and Grabowski, W. W.: Theoretical Formulation of Collision Rate and Collision Efficiency of Hydrodynamically Interacting Cloud Droplets in Turbulent Atmosphere, *J. Atmos. Sci.*, 62, 2433–2450, <https://doi.org/10.1175/JAS3492.1>, 2005.
- 455 White, B., Gryspeerdt, E., Stier, P., Morrison, H., and Thompson, G.: Uncertainty from the choice of microphysics scheme in convection-permitting models significantly exceeds aerosol effects, *Atmos. Chem. Phys. Discuss.*, 17, <https://doi.org/10.5194/acp-2016-760>, 2017.
- Wood, R., Field, P., and Cotton, W.: Autoconversion rate bias in stratiform boundary layer cloud parameterizations, *Atmos. Res.*, 65, 109–128, [https://doi.org/10.1016/s0169-8095\(02\)00071-6](https://doi.org/10.1016/s0169-8095(02)00071-6), 2002.
- Xue, L., Teller, A., Rasmussen, R., Geresdi, I., and Pan, Z.: Effects of Aerosol Solubility and Regeneration on Warm-Phase Orographic Clouds and Precipitation Simulated by a Detailed Bin Microphysical Scheme, *J. Atmos. Sci.*, 67, 3336–3354, <https://doi.org/10.1175/2010jas3511.1>, 2010.
- 460 Xue, L., Fan, J., Lebo, Z. J., Wu, W., Morrison, H., Grabowski, W. W., Chu, X., Geresdi, I., North, K., Stenz, R., Gao, Y., Lou, X., Bansemer, A., Heymsfield, A. J., McFarquhar, G. M., and Rasmussen, R. M.: Idealized Simulations of a Squall Line from the MC3E Field Campaign Applying Three Bin Microphysics Schemes: Dynamic and Thermodynamic Structure, *Mon. Weather Rev.*, 145, 4789–4812, <https://doi.org/10.1175/MWR-D-16-0385.1>, 2017.
- 465 Yang, F., Kollias, P., Shaw, R. A., and Vogelmann, A. M.: Cloud droplet size distribution broadening during diffusional growth: ripening amplified by deactivation and reactivation, *Atmos. Chem. Phys.*, 18, 7313–7328, <https://doi.org/10.5194/acp-18-7313-2018>, 2018.